Available online at www.sciencedirect.com

jmr&t Journal of Materials Research and Technology

www.jmrt.com.br

Original Article

Softening-precipitation interaction in a Nb-and N-bearing austenitic stainless steel under stress relaxation

Elivaldo Ribeiro Sá[a], *Samuel Filgueiras Rodrigues*[a,*], *Clodualdo Aranas Jr.*[b], *Fulvio Siciliano*[c], *Gedeon Silva Reis*[a], *José-María Cabrera-Marrero*[d,e], *Eden Santos Silva*[a,f]

[a] *Graduate Program in Materials Engineering, Federal Institute of Education, Science and Technology of Maranhão, Sao Luis 65075-441, Brazil*

[b] *Mechanical Engineering, University of New Brunswick, Fredericton, NB E3B 5A3, Canada*

[c] *Dynamic Systems Inc. 323 NY 355, Poestenkill, New York 12140, United States of America*

[d] *Department of Materials Science and Engineering, Universitat Politècnica de Catalunya, 08019 Barcelona, Spain*

[e] *Institute for Research in Metallrgy and Materials, Universidad Michoacana de San Nicolás de Hidalgo, 58030-Morelia, Michoacán, Mexico*

[f] *Federal Institute of Education, Science and Technology of Maranhão, Campus Barra do Corda, 65950-000, Brazil*

ARTICLE INFO

Article history:
Received 7 April 2020
Accepted 18 May 2020

Keywords:
Stress relaxation
Softening mechanism
Precipitation
Z-Phase
Austenitic stainless steel

ABSTRACT

In this work, stress relaxation technique was employed to analyze the softening-precipitation interaction in an ASTM F-1586 austenitic stainless steel, an alloy used in orthopedic implants. Hot compression tests were performed at temperature range of 800–1100 °C. Pre-strain of 5.0%, strain rate of 0.1 s^{-1}, and loading time exposure of 40 min were employed. The experiments were carried out in a dilatometer equipment. The stress-time (σ vs. log (t)) curves were plotted, and the microstructure of the specimens was characterized. The acquired results permitted to estimate the start (t_s) and the finish (t_f) times of the effective interaction between recovery and precipitation. The data revealed three distinct stages in the stress versus log time curves: (i) reduction in the stress levels due to static recovery; (ii) delay in the stress relaxation rate leading to a stress plateau, and (iii) sharp decrease of the stress levels associated with the finish of the precipitation. These results enabled the creation of Precipitation-Temperature-Time (PTT) curves for the present material. It was found that the onset time for the strain-induced Z-phase (CrNbN) is around 120 s and the precipitates delay the kinetics of the softening.

1. Introduction

Currently, millions of people in the world are affected by bone problems caused by fractures and degenerative and inflammatory diseases in joints. Materials like Ti-Co alloys are necessary

* *Corresponding author.*
E-mail: samuel.filgueiras@ifma.edu.br (S.F. Rodrigues).

https://doi.org/10.1016/j.jmrt.2020.05.066

Table 1 – The chemical composition of the ASTM F-1586 austenitic stainless steel (% mass).

C	Si	Mn	Ni	Cr	Mo	S	P	N	Cu	Nb	Fe
0.035	0.37	4.04	10.6	20.3	2.47	0.001	0.022	0.36	0.06	0.29	bal

to fix or replace the affected organ as permanent or temporary implants [1,2]. Among these alloys, ASTM F-1586 austenitic stainless steel has shown to be an alternative material due to its excellent mechanical properties to be applied as orthopedic components [3]. Although there are a number of previous studies regarding this material, the investigation related to the annealed condition and its mechanical strength lacks in-depth analysis. Researches have pointed out that the presence of complex carbonitrides in industrial processing has influenced the mechanical and corrosion properties of metallic materials [3,4]. Moreover, some investigations proposed new strategies to reduce the concentration of nickel and find the ideal concentration levels of chromium, niobium, manganese, and nitrogen for this type of austenitic stainless steel [5].

During the manufacturing process of implants such as hot forging, alloys undergo through microstructural evolution associated with softening phenomena. These metallurgical phenomena play an essential role in obtaining the final microstructure and the mechanical properties of the orthopedic components. In general, two softening mechanisms take place and control the physical response behavior during and after high-temperature deformation [6]. Those phenomena are known as recovery and recrystallization). When they occur during the deformation stage, they are named dynamic, while if they occur between deformation passes or after the final deformation, they are named static. In the particular case of highly alloyed steels, such as the present stainless steel, and depending on the deformation conditions (strain, strain rate and temperature), the typical softening mechanism are reduced to dynamic recovery (DRV), static recovery (SRX) and static recrystallization (SRX). In the case of microalloyed grades, precipitation can influence these mechanisms during the hot forming process, which has been of great interest to the metallurgical industry [7].

The influence of precipitates in delaying the austenite softening during the hot workability window has received considerable attention [8]. The thermomechanical process is drastically affected when complex precipitates are formed. These particles are capable of promoting different changes in the microstructure of the material when under deformation. Thus, Precipitation-Temperature-Time (PTT) diagrams have been introduced to show the relationship between the beginning and finish of precipitation. This approach has brought interesting interpretations regarding the kinetics of the softening mechanisms [9]. However, in some steels, this relationship is not well established due to the difficulty of determining which precipitates are forming under different processing conditions.

To date, several methods have been used to monitor the precipitation behavior during thermomechanical processing, among which the following stand out: i) microscopy analysis, ii) thermodynamic calculations, iii) microhardness measurement, iv) electrical resistivity measurement, and v) stress-strain curves analysis [10]. The microscopy analysis presents problems when the precipitates are very fine, leading to technical difficulties in separating and identifying them. The challenge with thermodynamic calculations is the approximations considering the ideal chemical activations, which can lead to overestimated values of the beginning and finish of precipitation [10]. Moreover, the stress-strain analysis is susceptible to experimental errors.

A mechanical technique to follow the softening-precipitation interaction and to determine the PTT curves of metallic materials was proposed by Liu & Jonas (Model L-J) [10]. The method is based on the stress relaxation curves analysis of the metal under hot compression tests. This procedure has been capable of predicting the start and finish times of strain-induced precipitation. To date, there is no study regarding the application of this technique for the investigation of the precipitates effect in some classes of austenitic stainless steel. Thus, the objective of the present work is to perform an in-depth examination of the softening-induced precipitation interaction through stress relaxation under hot compression of an ASTM F-1586. The presented results can be employed to improve the manufacturing process of this steel, which requires significant mechanical strength to act as an orthopedic implant within the human body without failure.

2. Material and methods

A rolled bar of an ASTM F-1586 austenitic stainless steel with 20 mm diameter was employed in this work. The chemical composition of this material is shown in Table 1 [11]. The bars were machined into cylindrical specimens of 5.0 mm diameter and 10 mm length. The softening-precipitation interaction was monitored via stress relaxation tests after small deformation under hot compression. The samples were initially heated to 1250 °C by induction process at a heating rate of 40 °C/s and held for 300 s to complete solubilization. The samples were then cooled down to the deformation temperature at a cooling rate of 5 °C/s. Hot compression tests were carried out at a temperature range 800–1100 °C, at a true strain of 0.05, and a strain rate of 0.1 s^{-1} under an argon atmosphere. In order to minimize friction, tantalum foils were used between anvils and samples. At the end of this cycle, the compression anvils were hold at fixed position for 40 min in a Bähr Thermoanalyse DIL 850 A/D Dilatometer while the temperature was hold constant (±0.5 °C). The samples were then water quenched to prevent appreciable diffusion of chromium and niobium atoms and to keep the solid solution unchanged. The employed thermomechanical process is presented in Fig. 1.

The samples were sectioned transversely in the direction of the applied load. Then, specimens were hot mounted in bakelite and polished using silicon carbide paper with grits of 400, 600, 800, 1000, and 1200 while being lubricated with water. Final polishing was carried out using diamond paste (3 μm and 1 μm) suspensions and a 0.02 μm colloidal silica suspension. The polished samples were then electrochemically

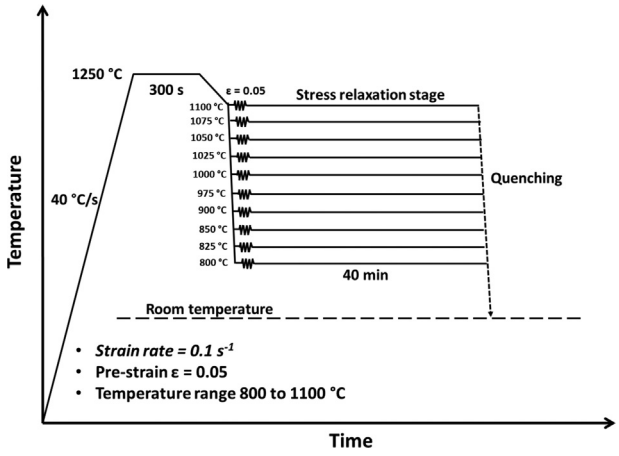

Fig. 1 – Schematic diagram showing the experimental procedure of the stress relaxation tests.

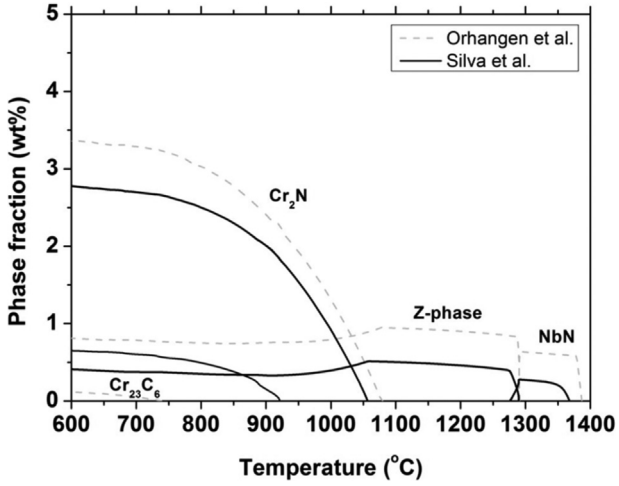

Fig. 2 – Thermodynamic calculation of the ASTM F-1586 austenitic stainless-steel phase diagram through FactSage 6.1.

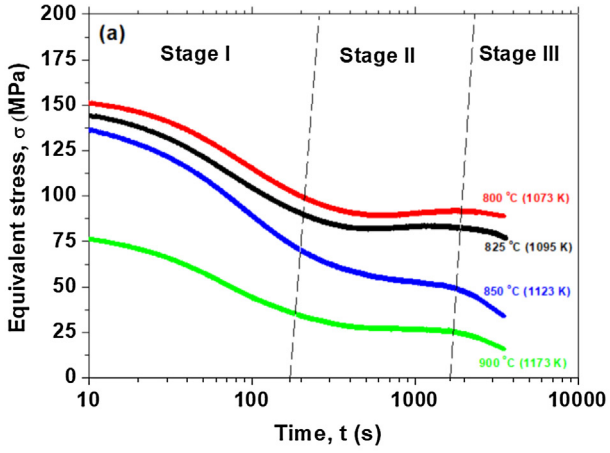

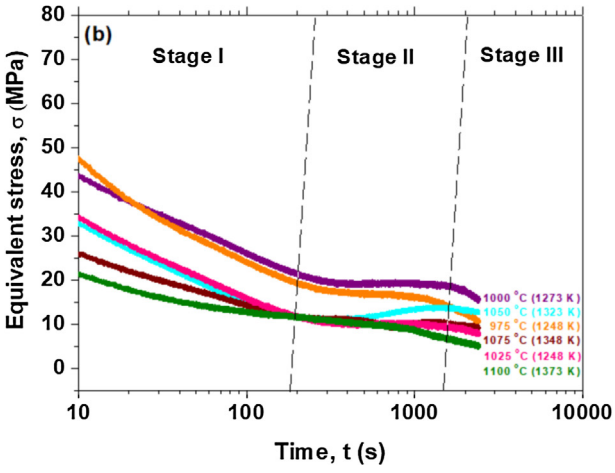

Fig. 3 – Stress relaxation curves acquired after 5.0% deformation of an ASTM F-1586 austenitic stainless steel, a) 800 °C < T < 900 °C, (b) 975 °C < T < 1100 °C.

etched using 65% nitric acid (HNO_3) and electrical current density of 1.0 A/cm^2, for approximately 10 s. The microstructural analysis was carried out using scanning electron microscopy (SEM). Details of the presence of precipitate particles and analytical mechanical analysis were investigated by examining the σ vs. log (t) curves. To validate the observations, dispersive energy spectroscopy (EDS) and thermochemical calculations via Factsage 6.1 software, at different stages of the stress relaxation test were performed.

3. Results and discussion

3.1. *Phase diagram*

The phase diagram of the present material was obtained through thermodynamic calculations using the Facstage 6.1 software and is shown in Fig. 2. It suggests that the Z-phase acts in the softening kinetics within the workability window of the thermomechanical process for the manufacturing of orthopedic implant parts. Analogous equilibrium diagram was determined by Orhangen et al. [12] for a steel of similar composition, where the presence of the Z-phase is verified in the hot workability frontier, see Fig. 2.

3.2. *Stages of stress relaxation curves*

The equivalent stress-log(t) curves obtained from the stress relaxation tests are shown in Fig. 3a) and b). The results revealed three distinct stages: *Stage I*, a short time after pre-strain, the curves start to reflect a considerable reduction in the stress level of approximately 40 MPa in an interval of 100 s (varies with temperature). *Stage II*, after approximately 120 s, the formation of stress levels plateau on the curves start to appear. This observation is an indication that a mechanism delaying the decrease of the stress relaxation is under evolution. An almost constant stress value is observed until a specific time that leads to the next stage. *Stage III*, after a longer time, t > 1800s, the curves restore their first behavior presenting in this way a more pronounced decrease of the stress levels. Here the effective mechanism which acted in the pre-

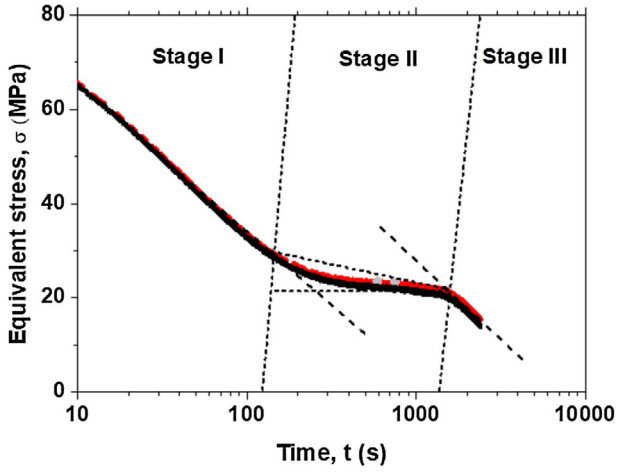

Fig. 4 – Typical stress relaxation curve showing the applied technique to obtain the coefficient and revealing the dependence in stages I and III. The sample has a pre-strain of 0.05 at 1000 °C.

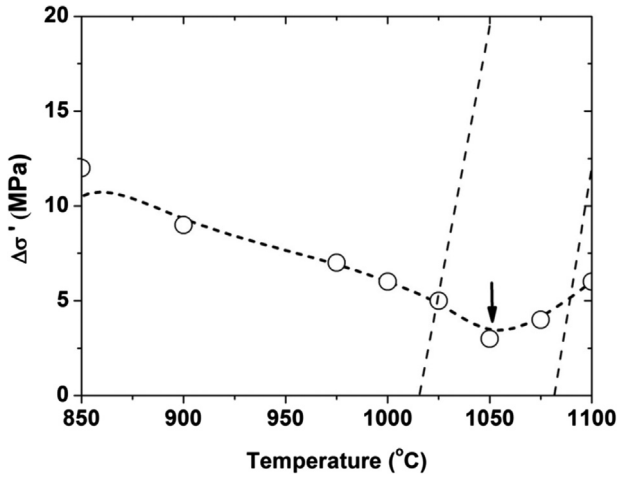

Fig. 5 – The dependence of the accumulation of stress (Δσ) on temperature in Stage II obtained from σ vs. log (t) curves.

vious stage may probably had been finished on the stress-log (t) curves.

The rise of the different stages, even with fluctuations in the initial stress (σ_o) appears as result of joint actions of, static recovery, static recrystallization and induced precipitation phenomena. These are the main causes of the stress level variations as time goes by. In *Stage I*, the reduction of the stress is due to the static recovery resulted from the energy stored during straining. As time passes, the dislocation density is reduced and has its distribution changed. In addition, the moderate value of the stacking fault energy of this steel, $\gamma_{SFE} = 69\,mJ/m^2$ [13], favors the static recovery mechanism hindering the simultaneous action of another thermally activated mechanisms such as static recrystallization. In *Stage II*, the plateaus in stress levels are due to the balance of the stress relaxation rate and the kinetics of the strain-induced precipitation. This behavior starts to appear after a specific incubation time, t > 120 s, suggesting that the occurrence of precipitation slows down the progress of stress relaxation. This is further discussed in section 3.6 where microscopy techniques were used. These results agree with previously reported researches done in microalloyed steels [14].

3.3. *Method for estimating the stress relaxation coefficient as a function of temperature*

The stress relaxation curve acquired after pre-strain of 0.05 at 1000 °C, is shown in Fig. 4. Here, linear dependence in stages I and III is clearly revealed. It is noticeably that the changes in stress (σ) with time (t) during the relaxation experiments fall in a linear relationship on a logarithmic time scale, according to Eq. 1, proposed by Liu & Jonas [15].

$$\sigma = \sigma_o - \alpha \ln(1 + \beta.t) + \Delta\sigma' \quad (1)$$

where σ_o is the initial stress (for t = 0 s), $\Delta\sigma'$ is the stress increment and α and β are experimental constants derived from the adjustments. The points at which Δσ deviates from zero and where Δσ is maximum are identified as the precipitation start (t_{ps}) and finish (t_{pf}) times, respectively.

The experimental adjustments of α =0.20 MPa and β = 0.30 s^{-1} showed good empirical relationships for Fig. 4. These values were obtained by adjusting the stress relaxation curves, using Eq.1. This indicates that the stress relaxation rate is due to the extrapolation and slope of the σ x log (t) curves. Some values reported in the literature for C-Mn and Ti-microalloyed steels (α =2.5 MPa, $\beta = 13\ s^{-1}$) [10] are well above the ones found here. It is believed that in Stage II, the possible occurrence of precipitation causes a decrease of the stress relaxation rate due to the interactions of the precipitates mainly in the grain boundaries under static recovery (SRV). This argument justifies the different slopes on the σ x log (t) curves and the delays in the stress relaxation rate, which depends on temperature and time. A technique proposed by Park et al. [16] relates an indirect detection of precipitation in austenite with the stress gradient between stages I and III in stage II. They investigated the volume fraction of precipitates of Nb(CN) in an austenitic stainless steel using this methodology. The results found in the present research are presented in Fig. 5.

As mentioned above, the behavior of the stress relaxation curves (see Fig. 3) showed remarkable peculiarities. One of those is Stage II, with the formation of plateaus in the stress levels as a consequence of a slight reduction of this resistance as the relaxation time increases. This behavior characterizes a type of *stress relaxation coefficient* (β), which varies with temperature (see Eq. 2). This variable is an indication of the effective action of the precipitation on the softening fraction, see Fig. 6. This variation in the value of β indirectly describes the progression of the precipitates volumetric fraction formed during stress relaxation, as reported by Djahazi et al. [17]. These results assume that the highest incidence of induced precipitation occurs close to 1050 °C. There is a temperature range where precipitation is more active in delaying the softening mechanisms. The precipitates reduce their effect by having a

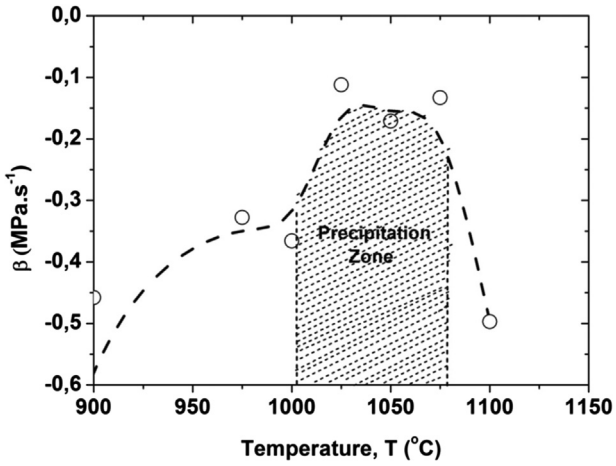

Fig. 6 – The dependence of the stress relaxation coefficient (β) on the temperature.

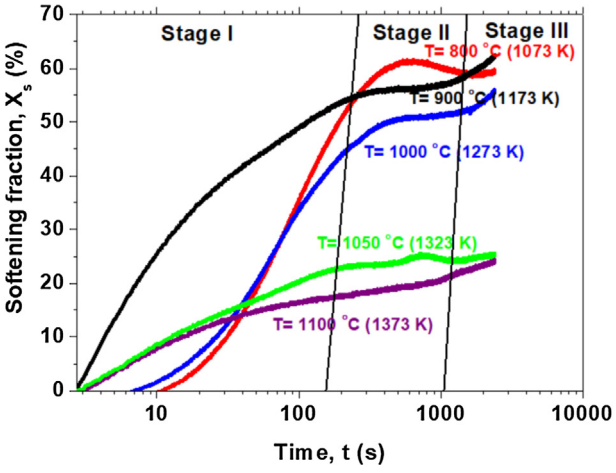

Fig. 7 – The softening fraction curves (X_s) vs. time (t) from stress relaxation.

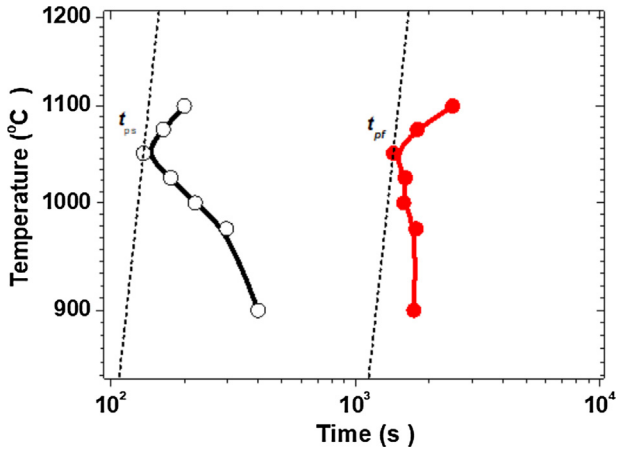

Fig. 8 – The PTT diagram of the ASTM F-1586 steel obtained by stress relaxation technique.

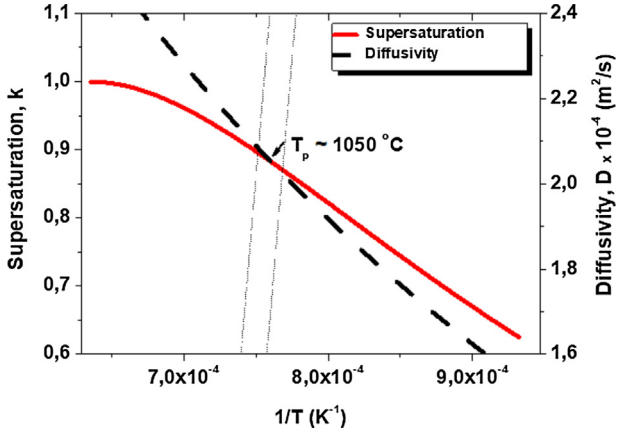

Fig. 9 – The supersaturation ratio ($k = k_s/k_T$) and diffusion ($D = D_o exp(-Q/RT)$) competition of the Z-phase (CrNbN) induced by hot deformation in stress relaxation.

low diffusivity at lower temperatures, and experiencing supersaturation and coalescence at higher temperatures.

$$\beta = \left[\frac{\partial(\Delta\sigma)}{\partial(\Delta \log t)}\right]_{T,\dot{\varepsilon}} \quad (2)$$

3.4. *Softening fraction by stress relaxation technique*

From the stress relaxation curves shown in Fig. 3, it is possible to estimate the softening fraction (X_s) as a function of time (t) in the three different stages of the σ vs. log (t) curves. This can be done through analytical equations, as proposed by Karjalainen et al. [18,19]. Here, they consider a rule of mixtures methodology composed of hardening and softening mechanisms represented in Eq. 3.

$$X_s = \frac{[(\sigma_1 - \alpha_1 \log t) - \sigma_t]}{[(\sigma_1 - \sigma_2) - (\alpha_1 - \alpha_2)\log t]} \quad (3)$$

where σ_1, σ_2, α_1 and α_2 are constants determined in stages I and III of the σ vs. log (t) curves in Fig. 4 and σ_t is the stress at a given time t.

The dependence of the softening fraction (X_s) on time (t) of stress relaxation at different temperatures is depicted in Fig. 7. Here, one can perceive that the curves have a sigmoidal shape, typical of materials that soften by simultaneous recovery and static recrystallization. It is noted that at lower temperatures ($T < 1000\,^{\circ}C$), the softening is prolonged and the delay in the softening fraction occurs up to times longer than 1000s due to the formation of the plateaus in *Stage II*. However, in conditions of high temperature ($T > 1025\,^{\circ}C$), the delay in the softening occurs is accelerated. This effect is already observed on the curves above, this takes place at approximately 120 s.

The behavior in *stage I* is due to the static recovery (SRV) of the material, which has a moderate stacking fault energy (γ_{SFE}), reducing in this way the action of thermally activated mechanisms. In *Stage II*, the competition between the kinetics of the softening during stress relaxation and the formation of strain-induced precipitates is responsible for the formation of the plateau. The delay in the softening fraction (X_s) is due to the prevention of the grains mobilities by precipi-

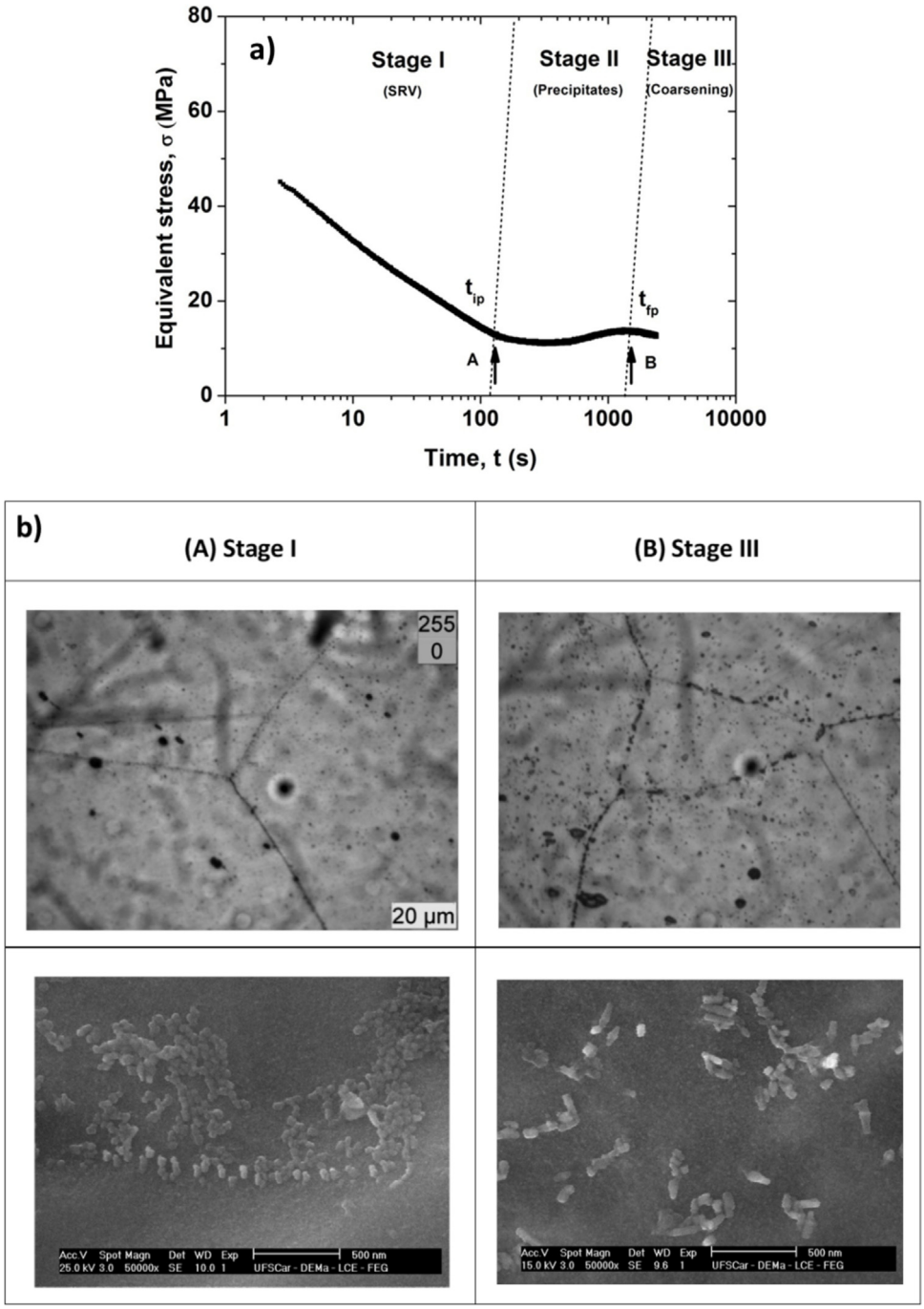

Fig. 10 – Plot of the a) stress relaxation curve at a temperature of 1025 °C showing the main regions analysed and the b) microstructural aspect of the Z-phase precipitates evolution obtained via OM and SEM in stages I and III. A) Nucleation of precipitates (clusters) and B) Coalescence of precipitates.

tate particles, as reported by Liu et al. [10,15]. In addition, at low temperature condition, the diffusivity of the chromium and niobium elements is limited. Therefore, a longer time for migration and agglomeration of atoms that form the precipitates is required, which restricts the softening fraction. These results are also consistent with previous studies reported by Giordani et al. [20]. They investigated a steel with a similar composition by employing a double pass hot torsion test. The static recovery and recrystallization (SRV-SRX) competitions were studied, and they concluded that the differences in the amount of applied strain change the initial time for the onset of the softening and precipitation phenomena [20,21].

3.5. *Determination of PTT curves by the stress relaxation method*

The times of start (t_{ps}) and finished of precipitation (t_{pf}) were estimated from the stress relaxation curves and are presented

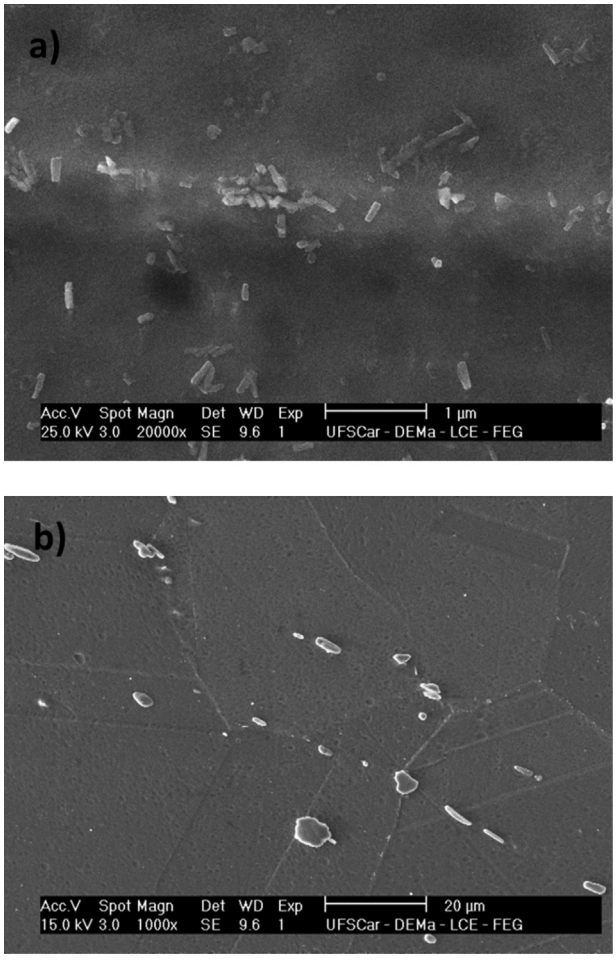

Fig. 11 – a) Fine and b) coarse precipitates of the Z-phase (CrNbN) that form in the grain boundaries during the stress relaxation test (Stage II), T =1050 °C.

in the form of PTT (Precipitation-Time-Temperature) diagram in Fig. 8. The PTT diagram shows that the nose of the curve is around 1050 °C with an incubation time of approximately 120 s. Here the condition of diffusion and supersaturation favors precipitation with less time. It can also be seen in the diagram that longer times are needed to start the precipitation, both below and above the nose.

The type C curve in the PTT diagram appears due to the competition between the driving force for precipitation and the diffusion mechanism of the chromium and niobium. The driving force for precipitation is the chemical free energy, the magnitude of which depends on the degree of supersaturation of the microalloying elements, and the driving force for diffusion is the chemical potential. In other words, it is the Gibbs energy variation of the elements in the solid solution [21]. At high temperature conditions (T > 1050 °C), below the solvus line (T =1300 °C), the atomic diffusion increases, and supersaturation decreases. These have a significant effect on the static recovery intervention, leading to a reduction in the stress levels (*Stage I*). Under these conditions, the precipitation rate is low, the solution is slightly supersaturated, and the decrease in free energy resulting from precipitation is also low [22]. However, at lower temperatures, the difference in the affinity of the chromium and niobium is one of the main reasons for the reduction in stress relaxation. Here, the dislocations require greater strength to move [23]. In either case, the time required for precipitation will increase, as shown in the PTT curves. Finally, for longer relaxation times, precipitates form and grow by diffusion. In these conditions, the precipitates coalesce sufficiently at the same time that the softening progresses, leading to the reduction of the stress levels (*Stage III*).

Another important variable to be considered is the Z-phase precipitation potential (CrNbN). This is given by the solubility product through the calculation of the supersaturation coefficient (k_s) of the microalloyed elements. The temperature and the amount of dissolved elements [Cr][Nb][N] during reheating at equilibrium temperature are taken into account. Giordani et al. [24] proposed a mathematical relation after the extraction technique of Z-phase precipitate has been used for each solubilization temperature. In their work, they considered that all the niobium present in the alloy precipitates as Z-phase. The relation is expressed by Eq. 4.

$$\log\left\{[Cr][Nb][N]\right\} = 7.557 - \frac{12277}{T(K)} \quad (4)$$

The importance of this equation stems from the fact that it is possible to determine and improve the amount of Z-phase precipitates present in the alloy microstructure at a given temperature (supersaturation coefficient, k_T). In addition, it is possible to determine the solubility temperature (T_s ~1290 °C) or even the ideal concentration of niobiumin in the alloy so that the complete solubility of the Z-phase could be achieved at a given temperature [25]. The competition between the diffusion kinetics of the Z-phase precipitates and the supersaturation degree under the imposed conditions is displayed in Fig. 9. This method was initially introduced by Dutta and Sellars [26]. Here it is also observed that the most favorable temperature under the applied conditions for the precipitation in the studied steel is around 1050 °C. Studies report that the critical value of supersaturation for the nucleation of solubilized austenite is about, $k_s = 4.8$ [27,28]. This value is considered to be in the upper range, and this variable is another factor that should be accounted for the driving force to precipitation. With the applied 0.05 pre-strain, the stored energy increases, leading to a higher thermodynamic potential for softening. This also increases the number of nucleation sites favoring Z-phase precipitation bringing down the values of supersaturation to $k_s = 2.2$. These values are below those reported in the literature for niobium microalloyed steels with precipitation of Nb(CN), $5.0 < k_s < 8.0$ [29]. Temperatures below 1100 °C favor the precipitation of the Z-phase in the solid solution. The solubilities of chromium and niobium in austenite drop substantially below this temperature and the chromium, with higher concentration, is removed from the matrix. These findings were reported by Sousa et al. [30]. They showed that these precipitates could decrease the mechanical strength of the steel.

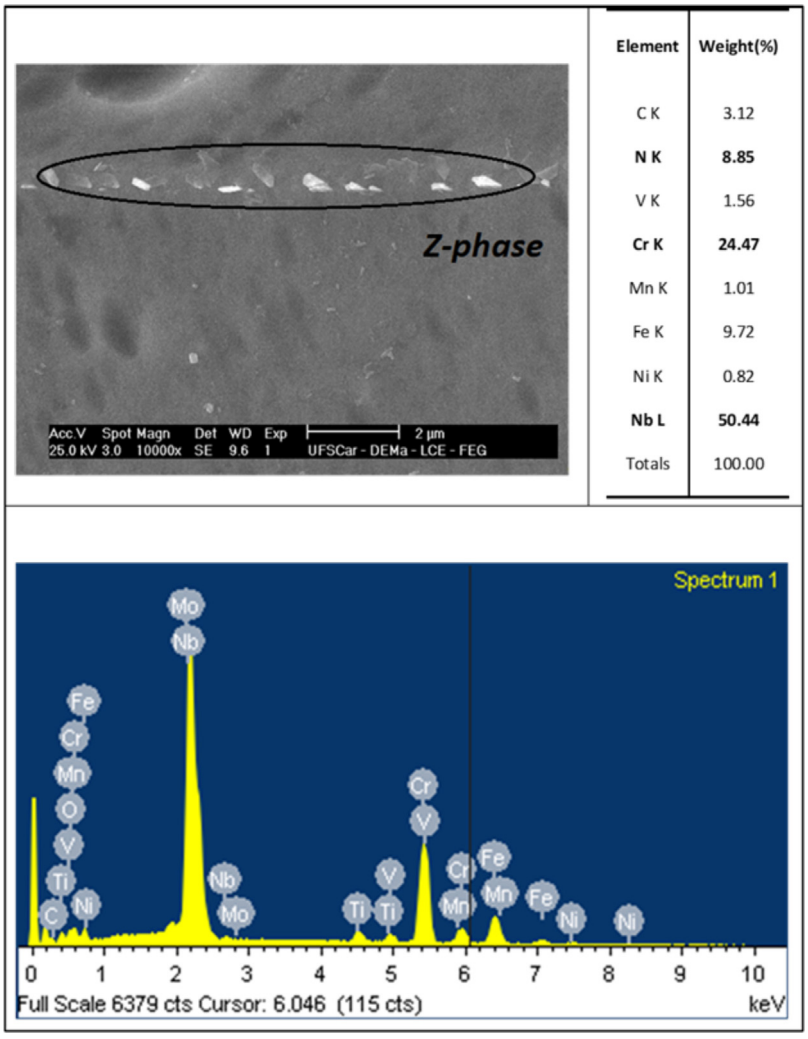

Fig. 12 – The SEM/EDS analysis of the Z-phase precipitates (CrNbN) present in the grain boundaries captured in stage III at 1050 °C.

3.6. *Microstructural behavior*

The precipitation kinetics could be estimated from the start to the finish corresponding to the plateau stage in the stress relaxation curves (see Fig. 3). The microstructural behavior at these two points was validated via scanning electron microscopy, see Fig. 10a) and b). The image suggests that the precipitation in the austenitic matrix occurs in the interior and along the grain boundaries. Different size, distribution, and morphology over time in Stage II can also be seen. It is also observed that precipitation takes at least 120 s to start an effective process.

The SEM analysis shown in Fig. 10b) and Fig. 11 reveals that clusters of fine particles smaller than 20 nm are observed at the onset of precipitation. They are nucleated heterogeneously in the grain boundaries. These tiny particles are effective in delaying the stress relaxation rate. As time goes by, precipitates start to coalesce, increasing their size to 125 nm at the finish of Stage II. The coalescence forming larger precipitates contributes to the stress levels decrease, and the quantity of these particles also decreases. The coalescence of the Z-phase precipitates is directly related to the surface tension of the matrix-precipitate interface. This observation is due to the contour surface energy, where the free energy per atom of a large precipitate is lower than that of a small one. This free energy difference is the driving force that causes the dissolution of small precipitates and the growth of larger ones. Similar results have been reported by Liu et al. [31] when studying the kinetics of Nb(CN) precipitation in Nb microalloyed steels. These observations support the interpretation that the formation of the present strain-induced Z-phase precipitates during the progress of stress relaxation is responsible for the formation of the plateaus in the σ vs. log (t)curves.

The MEV/EDS analysis of Z-phase precipitates (Nb, 24.47% Cr, 8.85% N) is shown in Fig. 12. The particles nucleate and grow in the grain boundaries, as mentioned above, and is shown in Fig. 11. These precipitates prevent grain boundary mobility, delaying the ability to static recovery and recrystallization. Researches report that these precipitates are complex carbonitrides with a tetragonal structure formed by chromium, niobium and nitrogen that stabilize the austenitic phase in stainless steels [32,33]. The formation process of these precipi-

tates is not clearly explained, but they present relative stability when compared to other carbonitrides. Finally, when the stage III is reached, after a specific time (t > 30 min) with the coalescence and dissolution of the precipitates, there is a better redistribution of the grain boundaries and larger precipitates. This phenomenon led to significant relief of the stress levels.

4. Conclusions

In the present investigation, the behavior of the static recovery-precipitation interaction during stress relaxation tests was evaluated. The start (t_{ps}) and finishing (t_{pf}) time of the strain-induced Z-phase precipitation (CrNbN) in ASTM F steel-1586 were established. The results led to the following conclusions:

1 The stress relaxation technique allows the indirect investigation to monitor the precipitation process through the stress levels in the σ vs. log (t) curves. Three different stages were revealed, and a delay in stress relaxation was observed in the second stage.
2 After the 0.05 pre-strain, during the relaxation period, a time of approximately 120 s was necessary to observe the curve profile change from a decreasing behavior to a plateau. This behavior suggests the required time for sufficient precipitation of the Z-phase. Additionally, the proposed PTT diagram showed a curve C-type form, a characteristic of the softening-precipitation competition. The effective precipitation started around 1050 °C after the confirmed time of approximately 120 s.
3 The microstructure analysis showed that the precipitates are of the type (CrNbN), and at the start of the effective precipitation process, they have sizes of about 20 nm and coalesce into larger particles (125 nm) reducing their number in the matrix at the finish of the second stage. These bigger precipitates relieve the delay of the stress relaxation leading to the continuation of the static recovery.

Conflictof interests

The authors declare no conflict of interest.

Acknowledgments

The authors are grateful for the financial support from the Research and Support Foundation of Maranhão (FAPEMA), CAPES and CNPq. JMC thanks CONACyT (Mexico) the partial funding of his sabbatical leave at UMSNH. They are grateful to Ana Hernandez from Universidad Politecnica de Catalunya (UPC) and Fundació CTM Centre Tecnologic Barcelona, Spain, for her support in the stress relaxation tests. **The authors also** acknowledge the funding received from the Natural Sciences and Engineering Research Council of Canada (NSERC), Canada Foundation for Innovation (CFI), New Brunswick Innovation Foundation (NBIF) and the Harrison McCain Foundation.

REFERENCES

[1] Navarro M, Michiardi A, Castaño O, Planell JA. Biomaterials in orthopaedics. J R Soc Interface 2008;5(27):1137–58, http://dx.doi.org/10.1098/rsif.2008.0151.
[2] Hench LL, Polak JM. Third-generation biomedical materials. Science 2002;295:1014–7, http://dx.doi.org/10.1126/science.1067404.
[3] Lo KH, Shek CH, Lai JKL. Recent developments in stainless steels. Mater Sci Eng R 2009;65:39–104, http://dx.doi.org/10.1016/j.mser.2009.03.001.
[4] Mataya MC, Perkins CA, Thompson SW, Matlock DK. Flow stress and microstructural evolution during hot working of alloy 22cr-13ni-5mn-0.3n austenitic stainless steel. Metal Mater Trans A 1996;27:1251–66, http://dx.doi.org/10.1007/BF02649862.
[5] Ibrahim MZ, Sarhan AAD Yusuf F, Hamdi M. Biomedical materials and techniques to improve the tribological, mechanical and biomedical properties of orthopedic implants – a review article. J Alloy Compd 2017;714:636–67, http://dx.doi.org/10.1016/j.jallcom.2017.04.231.
[6] Rollett A, Humphreys F, Rohrer GS, Hatherly M. Recrystallization and related annealing phenomena. 2nd. ed. Imprint: Pergamon; 2004, eBook ISBN: 9780080540412.
[7] Robinson PW, Jack DH. Precipitation of z-phase in a high-nitrogen stainless steel. J Heat Treat 1985;4:69–74, http://dx.doi.org/10.1007/BF02835491.
[8] Palmiere EJ, Garcia CI, DeArdo AJ. The influence of niobium supersaturation in austenite on the static recrystallization behavior of low carbon microalloyed steels. Metall Mater Trans A 1996;27:951–60, http://dx.doi.org/10.1007/BF02649763.
[9] Dutta B, Palmiere EJ, Sellars CM. Modelling the kinetics of strain induced precipitation in Nb microalloyed steels. Acta Mater 2001;49:785–94, http://dx.doi.org/10.1016/S1359-6454(00)00389-X.
[10] Liu WJ, Jonas JJ. A stress relaxation method for following carbonitride precipitation in austenite at hot working temperatures. Metall Mater Trans A 1988;19:1403–13, http://dx.doi.org/10.1007/BF02674014.
[11] International organization for standardization (ISO) 5832-5839; Implants for surgery - metallic materials–part 9: wrought high nitrogen stainless steel; 2007. p. 4. Switzerland.
[12] Örnhagen C, Nilsson JO, Vannevik H. Characterization of a nitrogen-rich austenitic stainless steel used for osteosynthesis devices. J Bio Mater Res 1996;31:97–103, http://dx.doi.org/10.1002/(SICI)1097-4636(199605)31:1<97::AID-JBM12>3.0.CO;2-J.
[13] Giordani EJ, Jorge AM Jr, Balancin O. Proportion of recovery and recrystallization during interpass times at high temperatures on a Nb- and N-bearing austenitic stainless-steel biomaterial. Scrip Mater 2006;55:743–6, http://dx.doi.org/10.1016/j.scriptamat.2006.05.015.
[14] Palmiere EJ. Precipitation phenomena in microalloyed steels. Proc Conf Microalloying 95, Pittsburgh 1995. Iron and Steel Soc: 307-820.
[15] Liu WJ. A review of the stress-relaxation method for following the kinetics of precipitation, recovery and recrystallization. Mater Sci For 2012;706–709:2758–63.
[16] Park SH, Yue S, Jonas JJ. Continuous-cooling-precipitation kinetics of Nb(CN) in high-strength low-alloy steels. Metall Mater Trans A 1992;23:1641–51, http://dx.doi.org/10.1007/BF02804360.
[17] Djahazi M, He XL, Jonas JJ, Sun WP. Influence of boron on nature and distribution of strain induced precipitates in (Ti,Nb) high strength low alloy steels. Mater Sci Tech 1992;8:628–36, http://dx.doi.org/10.1179/mst.1992.8.7.628.

[18] Karjalainen LP, Perttula J. Characteristics of static and metadynamic recrystallization and strain accumulation in hot-deformed austenite as revealed by the stress relaxation method. ISIJ Int 1996;36:729–36, http://dx.doi.org/10.2355/isijinternational.36.729.
[19] Karjalainen LP, Perttula J, Xu Y, Proc Niu J. 7th int. Symp. On physical simulation of casting, Hot rolling and welding. Tsukuba, Ibaraki, Japan: National Research Institute for Metals; 1997. p. 231–6.
[20] Giordani EJ, Jorge AM Jr, Balancin O. Evidence of strain-induced precipitation on a Nb and N-bearing austenitic stainless steel biomaterial. Mater Sci For 2005;500:179–86, http://dx.doi.org/10.4028/www.scientific.net/MSF.500-501.179.
[21] Stüwea HP, Padilha AF, Siciliano JrF. Competition between recovery and recrystallization. Mater Sci Eng A 2002;333:361–7, http://dx.doi.org/10.1016/S0921-5093(01)01860-3.
[22] Monajati H, Zarandi F, Jahazi M, Yue S. Strain induced γ′ precipitation in nickel base superalloy udimet 720 using a stress relaxation based technique. Scrip Mater 2005;52:771–6, http://dx.doi.org/10.1016/j.scriptamat.2004.12.006.
[23] Gavriiljuk VG. Nitrogen in iron and steel. ISIJ Inter 1996;36:738–45, http://dx.doi.org/10.2355/isijinternational.36.738.
[24] Giordani EJ, Guimarães VA, Pinto TB, Ferreira I. Effect of precipitates on the corrosion–fatigue crack initiation of ISO 5832-9 stainless steel biomaterial. Inter J Fat 2004;26:1129–36, http://dx.doi.org/10.1016/j.ijfatigue.2004.03.002.
[25] Bernardes FR, Rodrigues SF, Silva ES, Reis GS, Silva MBR, Jorge AM Jr, et al. Analytical modeling of the thermomechanical behavior of ASTM F-1586 high nitrogen austenitic stainless steel used as a biomaterial under multipass deformation. Mater Sci Eng C 2015;51:87–8, http://dx.doi.org/10.1016/j.msec.2015.02.040.
[26] Dutta B, Sellars CM. Effect of composition and process variables on Nb(C,N) precipitation in niobium microalloyed austenite. Mater Sci Tech 1987;3:197–205, http://dx.doi.org/10.1179/mst.1987.3.3.197.
[27] Llanos L, Pereda B, López B. Interaction between recovery, recrystallization, and NbC strain-induced precipitation in high-Mn steels. Metal Mater Trans A 2015;46:5248–65, http://dx.doi.org/10.1007/s11661-015-3066-2.
[28] Wang Z, Sun X, Yan Z, Yong Z, Yong Q, Li Z, et al. Carbide precipitation in austenite of a Ti-Mo-containing low-carbon steel during stress relaxation. Mater Sci Eng A 2013;573:84–91, http://dx.doi.org/10.1016/j.msea.2013.02.056.
[29] Medina SF, Mancilla JE. Influence of alloying elements in solution on static recrystallization kinetics of hot deformed steels. ISIJ Int 1996;36:1063–9, http://dx.doi.org/10.2355/isijinternational.36.1063.
[30] Souza RC, Silva ES, Jorge AM Jr, Cabrera JM, Balancin O. Dynamic recovery and dynamic recrystallization competition on a Nb- and N-bearing austenitic stainless steel biomaterial: influence of strain rate and temperature. Mater Sci Eng A 2013;582:96–7, http://dx.doi.org/10.1016/j.msea.2013.06.037.
[31] Liu WJ, Jonas JJ. Ti(CN) precipitation in microalloyed austenite during stress relaxation. Metal Mater Trans A 1988;19:1415–24, http://dx.doi.org/10.1007/BF02674015.
[32] Erneman J, Schwind M, Liu P, Nilsson JO, Andren HO, Agren J. Precipitation reactions caused by nitrogen uptake during service at high temperatures of a niobium stabilised austenitic stainless steel. Acta Mater 2004;52:4337–50, http://dx.doi.org/10.1016/j.actamat.2004.06.001.
[33] Silva MBR, Cabrera JM, Balancin O, Moreira AM Jr. Thermomechanical controlled processing to achieve very fine grains in the ISO 5832-9 austenitic stainless steel biomaterial. Mater Char 2017;127:153–60, http://dx.doi.org/10.1016/j.matchar.2017.02.026.